Eur. J. Mineral., 32, 483–494, 2020
https://doi.org/10.5194/ejm-32-483-2020


European Journal of Mineralogy
Open Access

# Wumuite ($KAl_{0.33}W_{2.67}O_9$) – a new mineral with an HTB-type structure from the Panzhihua–Xichang region in China

**Yuan Xue[1,2], Guowu Li[1], and Yingmei Xie[1]**

[1]Crystal Structure Laboratory, Science Research Institute, China University of Geosciences (Beijing), Beijing 100083, China
[2]School of Materials Science and Technology, China University of Geosciences (Beijing), Beijing 100083, China

**Correspondence:** Guowu Li (liguowu@cugb.edu.cn)

Received: 26 February 2020 – Revised: 14 August 2020 – Accepted: 9 September 2020 – Published: 7 October 2020

**Abstract.** Wumuite, ideally $KAl_{0.33}W_{2.67}O_9$, is a new mineral species found in the Neoproterozoic Sinian light-weathered biotite–quartz monzonite in the southern part of the Panzhihua–Xichang region (Nanyang village: 26°46′8.21″ N, 101°27′13.86″ E), China. It is associated with quartz, orthoclase, albite, biotite, hornblende, kaolinite, ilmenite, goethite, hematite, zircon, zoisite, tourmaline, monazite-(Ce), allanite-(Ce), scheelite, tellurite, tewite, and an unidentified, potentially new mineral corresponding to $WO_3$. Wumuite occurs as light green hexagonal tabular crystals, is up to 0.3 mm in diameter, and has a vitreous to adamantine luster and a white streak; i.e., it is transparent. The mineral is brittle with good cleavage parallel to $\{10\bar{1}0\}$ and $\{0001\}$. It has a Mohs hardness of about 5–6 and a calculated density of 6.52 g cm$^{-3}$. Electron microprobe analyses yielded the following (in wt % – average of 10 spot analyses of one sample): $K_2O$ 5.55, $WO_3$ 91.16, $TeO_2$ 0.59, and $Al_2O_3$ 2.52, with a total of 99.82. The empirical formula for wumuite calculated on the basis of $O_{apfu} = 9$ is $K_{0.80}(W_{2.68}Al_{0.34}Te_{0.03})_{\sum 3.05}O_9$, ideally $K(W_{2.67}Al_{0.33})_{\sum 3}O_9$ or $KAl_{0.33}W_{2.67}O_9$. The strongest four diffraction lines [$d$ Å ($I$) ($hkl$)] are 6.261(36)(010), 3.727(30)(001), 3.161(100)(020), and 2.413(40)(021). Wumuite is hexagonal, in space group $P6/mmm$, with $a = 7.2952(5)$ Å, $c = 3.7711(3)$ Å, $V = 173.81(2)$ Å$^3$, and $Z = 1$. The crystal structure was solved and refined to a reliability factor of $R_1[F^2 > 4\sigma(F^2)] = 0.025$ ($wR_2 = 0.072$) based on 164 unique reflections (777 measured reflections, $R_{(int)} = 0.011$). Wumuite has a hexagonal tungsten bronze (HTB)-type structure. The layers of corner-sharing $[(W, Al)O]_6$ octahedra, with the layers oriented normal to the short (3.7713 Å) $c$ repeat and along with the W–O–W links, connect to form a hexagonal ring channel (tunnel). K is distributed in the hexagonal channel. An associated new mineral, tewite, which was discovered in the same area, also has a new tungsten bronze (TB)-type-related structure and has a genetic connection with wumuite in both back-scattered electron (BSE) images and synthetic experiments. The formation of wumuite is likely related to the nearby quartz-vein-type Au mineralization. The mineral was formed by a metasomatic reaction between W-rich hydrothermal fluids and the potassium feldspar in the monzonite.

## 1 Introduction

In 2014, we reported a new K–Te–W oxide mineral species, tewite (Li et al., 2019), discovered in the Neoproterozoic Sinian lightly weathered biotite–quartz monzonite in the southern part of the Panzhihua–Xichang region, Nanyang village, on the boundary between Panzhihua city, Sichuan Province, and Huaping County, Yunnan Province, China. During the further study of samples from this area, a new K–W mineral species with a hexagonal tungsten bronze structure, i.e., wumuite, was found in the same sample. This new mineral was named after the Wumu River near the source area, and the mineral species and its name have been approved by the International Mineralogical Association Commission on New Minerals, Nomenclature and Classification (IMA2017-067a). A type specimen of wumuite has been deposited in the collections of the Geological Museum of China, 15 Xisi Mutton Alley, Beijing, China, under registration number M13782 (holotype) and in the Crystal Structure Laboratory, China University of Geosciences, Beijing 100083, China, under catalogue number NY-6-2Z (cotype). The suggested Strunz classification is 04.E (metal: oxygen $\leq 1:2$), 04 oxides and hydroxides. The Dana's classification is 07 multiple oxides $AB_3O_9$.

## 2 Occurrence and paragenesis

The Pan–Xi (Panzhihua–Xichang) region, located on the western edge of the Yangtze Plate and within the inner zone of the Emeishan large igneous province, is one of China's important mineral resource areas, containing rare earths, niobium, tantalum, and magnetite related to magmatic rocks. Neoproterozoic diabases, ultramafic rocks, intermediate-silicic rocks, quartz diorite, and quartz monzonite are widely exposed in the crystalline basement rocks of this region. Among them, the Sinian intermediate-silicic and silicic volcanic rocks have a widespread distribution, with an outcrop area of about 1100 $km^2$ (Li, 2001). Permian Emeishan basalts, mafic–ultramafic rocks, syenite, and granite are also widely distributed in this region. Several vanadium–titanium magnetite deposits and sulfide deposits occur in the mafic–ultramafic rocks in which the famous Panzhihua vanadium–titanium magnetite deposit is distributed. In addition, a series of niobium–tantalum deposits and mineralized spots hosted in alkali granite and alkali pegmatite veins, which formed during the Indosinian period (Li, 2001), are distributed in the Pan–Xi region (Qin, 1995; He, 2004; Zhang et al., 2009). The ore-bearing alkali pegmatite veins are closely related to the syenite and granite masses that developed extensively in the Pan–Xi region and are strongly temporally and spatially linked to the Emeishan large igneous province (Zhong et al., 2007; Xu et al., 2008). An independent sulfide-type tellurium deposit, related to the hydrothermal activity, has been found in the sulfide ore in Dashuigou, Shimian County, northern Pan–Xi region, and the main tellurium mineral discovered in this deposit is tetradymite (Chen et al., 1994) (Fig. 1).

A new mineral, wumuite, was discovered in the southern part of the Panzhihua–Xichang region, near Nanyang village (26°46′18.21″ N, 101°27′13.86″ E) adjacent to the northwestern part of Panzhihua city, at the junction of Sichuan Province and Yunnan Province. The administrative division of this area belongs to Huaping County, Lijiang city, Yunnan Province. The mineral occurs at the edge of the Neoproterozoic Sinian intermediate-silicic rocks, near the contact zone of the Permian mafic rocks. The zircon age of the biotite-bearing quartz monzonite is 800 Ma. The rock is lightly weathered and fragile, forming boulders with occasional fresh remnant cores. Moreover, the rock is yellowish gray with an aplitic texture. Its main minerals include plagioclase (45 %), orthoclase (30 %), quartz (10 %–25 %), biotite (5 %–10 %), and hornblende (5 %). Extremely rare grains of wumuite were found in the heavy mineral concentrates. The minerals associated with the wumuite include orthoclase, albite, biotite, hornblende, kaolinite, ilmenite, goethite, hematite, zircon, zoisite, tourmaline, monazite-(Ce), allanite-(Ce), scheelite, tellurite, tewite, and an unnamed mineral $WO_3$.

Approximately 300 m southwest of the discovery site, there is a pyrite-quartz-vein-type gold deposit in a fault zone in the mafic rock mass (gabbro), and the fault extends into the vicinity of the locality of the tewite and wumuite. The origin of the wumuite may be related to the gold mineralization in this area. It is speculated that it may have been formed by the tungsten-containing hydrothermal fluids intercalating into the monzonite and reacting with the potassium feldspar.

## 3 Appearance and physical properties

Wumuite occurs as a light green tabular crystal, up to 0.3 mm in diameter, with a vitreous to adamantine luster; has a white streak; and it is transparent (Fig. 2). The ideal crystal forms are major {0001}, with minor $\{10\bar{1}0\}$, $\{01\bar{1}0\}$, and $\{1\bar{1}00\}$ (Fig. 3). The mineral is brittle with good cleavage planes parallel to $\{10\bar{1}0\}$ and {0001}. It has a Mohs hardness of about 5–6 and a calculated density of 6.52 $g\,cm^{-3}$. Optically, wumuite is uniaxial (+). The Gladstone–Dale relationship and the chemical constituent predict an average refraction index of 2.13.

As shown in the back-scattered electron (BSE) images (Fig. 2b–d), scheelite and tewite were identified in the wumuite crystal. The scheelite particles in the wumuite have a relatively automorphic appearance, indicating that they formed earlier than the wumuite, while the tewite is distributed among the particles of wumuite, suggesting that it may have formed later than the wumuite (Fig. 2d).

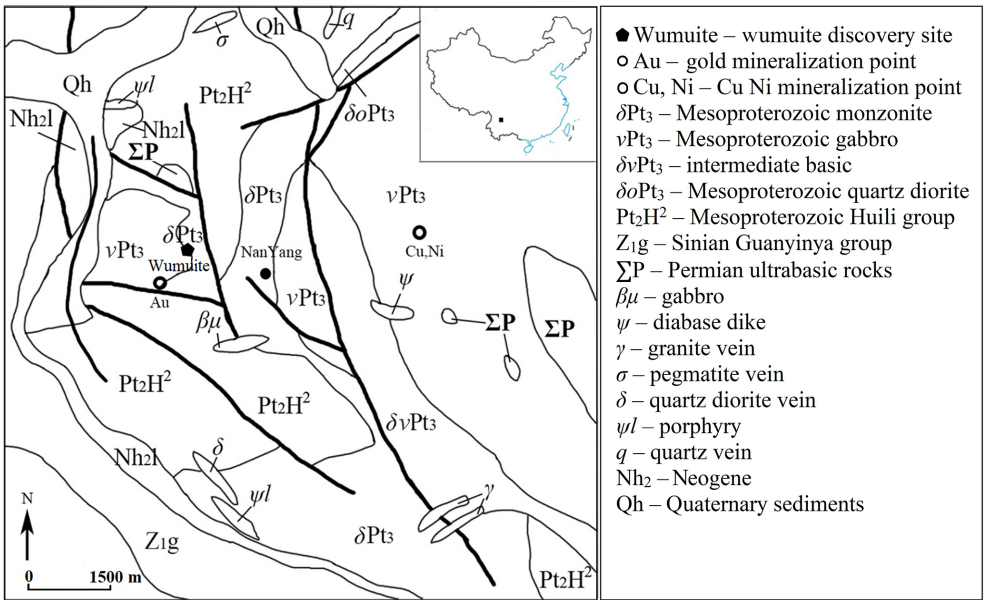


**Figure 1.** Geologic map of the type locality.

**Table 1.** Chemical data (in wt %) for wumuite.

| Constituent | Mean | Range | SD | Probe standards |
|---|---|---|---|---|
| $Al_2O_3$ | 2.52 | 2.40–2.68 | 0.04 | albite |
| $WO_3$ | 91.16 | 88.45–92.35 | 1.10 | scheelite |
| $K_2O$ | 5.55 | 5.16–5.85 | 0.28 | microcline |
| $TeO_2$ | 0.59 | 0.54–0.75 | 0.08 | $Sb_2Te_3$ |
| Total | 99.82 | | | |

## 4 Chemical composition

The chemical composition of the wumuite was determined using a JEOL JXA-8100 electron microprobe, operated in the wavelength-dispersive mode, with the following conditions: 20 kV, 10 nA, and an electron beam diameter of 2 µm. Analytical data from 10 points on one grain are presented in Table 1. The empirical formula calculated on the basis of $O_{apfu} = 9$ is $K_{0.80}(W_{2.68}Al_{0.34}Te_{0.03})_{\sum 3.05}O_9$. The simplified end formula is $K(W_{2.67}Al_{0.33})_{\sum 3}O_9$ or $KAl_{0.33}W_{2.67}O_9$. The empirical chemistry agrees with the general formula $K_x(W_{3-x/3}Al_{x/3})_{\sum 3}O_9$, with $x \leq 1$. Similar to general tungsten bronze structural materials, wumuite exhibits nonstoichiometric characteristics. In order to balance the valence, replacement of $W^{6+}$ by $Al^{3+}$ is necessary. The chemical composition suggests a substitution of $3\square + W^{6+} = 3K^{+} + Al^{3+}$, corresponding to a solid solution towards $KAl_{0.33}W_{2.67}O_9$.

## 5 Infrared spectra

An infrared (IR) spectrum of wumuite (Fig. 4) was collected using a Bruker HYPERION 1000 FTIR microscope, which was operated in reflection mode, and the spectrum data were processed using the OPUS software. A polished face of a single crystal particle was used, and a silver reflective background correction was applied. The spectrum in the region of 4000–400 $cm^{-1}$ was acquired during 32 cycles at a resolution of 4 $cm^{-1}$. The IR absorption band at 816 $cm^{-1}$ represents stretching modes of the $WO_6$ octahedron, and the bands at 523, 475, 446, and 424 $cm^{-1}$ represent the W–O bending vibrations (Gadsden, 1975).

## 6 X-ray diffraction and crystal chemistry

### 6.1 Powder diffraction

The powder X-ray diffraction data were acquired with a Rigaku Oxford diffraction XtaLAB PRO-007HF (Mo$K\alpha$, 50 kV, 24 mA) (Table 2). The four strongest X-ray powder diffraction lines [$d$ in Å ($I$) ($hkl$)] are 6.261(36)(010), 3.727(30)(001), 3.161(100)(020), and 2.413(40)(021), which are similar to the synthetic material, i.e., $K_{0.33}(W_{0.89}Al_{0.11})_{\sum 1}O_3$ (ICDD, 2020b), with slightly different peaks assigned to (001) and (002) and additional weak peaks at 29.37 and 32.88°. The unit-cell parameters refined from the powder diffraction data using the CHECKCELL software are as follows: $a = 7.285(5)$ Å, $c = 3.767(1)$ Å, and $V = 173.1(3)$ Å$^3$, which are consistent with the single-crystal results.

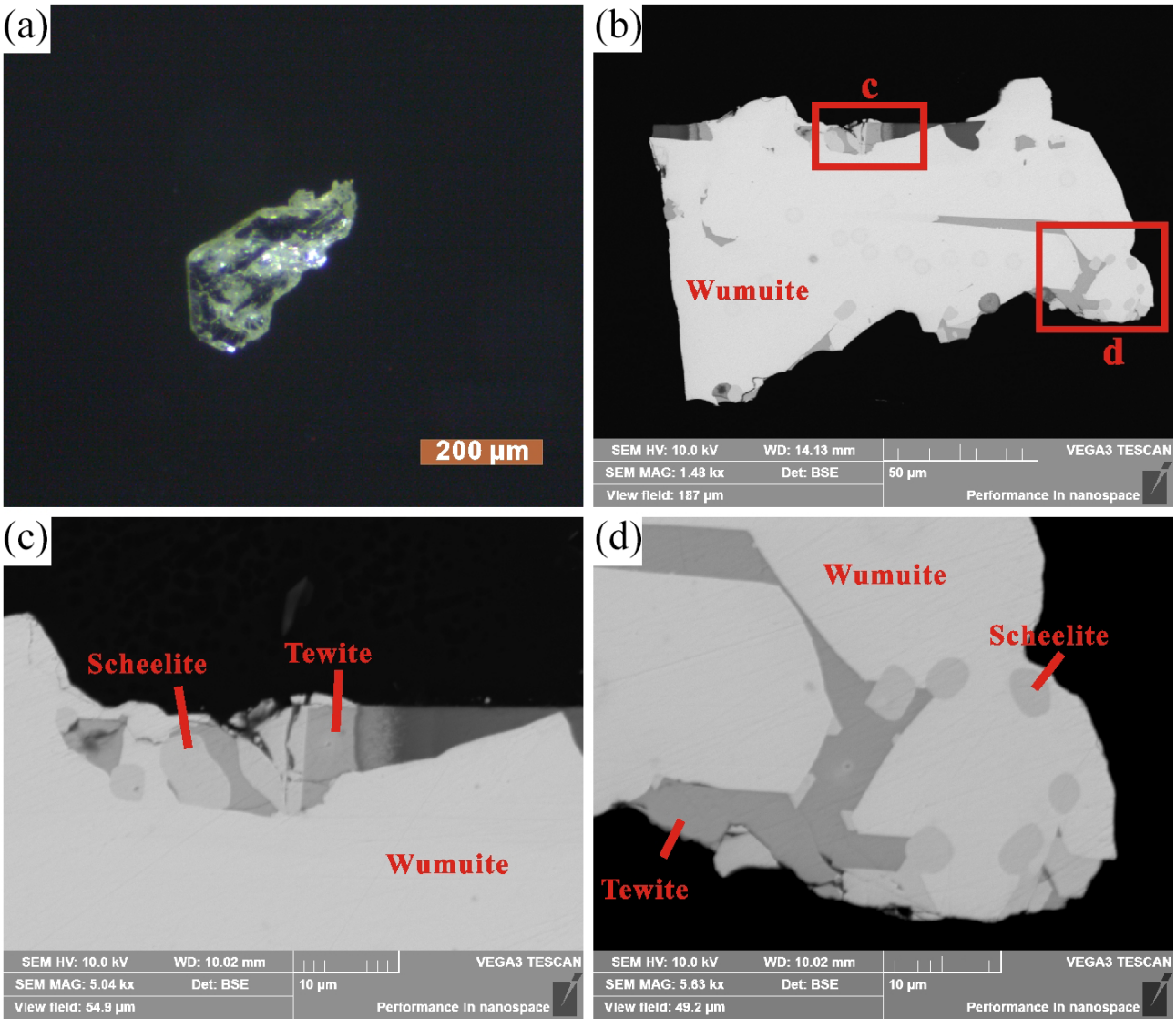


**Figure 2.** Backscattered electron (BSE) images of wumuite and some associated minerals.

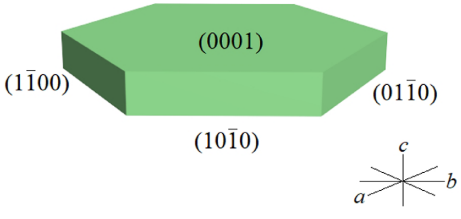


**Figure 3.** Ideal crystal form of wumuite.

### 6.2 Single-crystal structure refinement

Single-crystal X-ray studies were carried out twice. The first study involved the use of a Bruker Apex-CCD single-crystal X-ray diffractometer with a CCD detector and a Mo$K\alpha$ X-ray source (45 kV, 35 mA), which yielded the following results: $a = 7.2952(5)$ Å, $c = 3.7711(3)$ Å, $V = 173.81(2)$ Å$^3$, and $Z = 1$. The second study used a Rigaku Oxford diffraction XtaLAB PRO-007HF rotating anode microfocus X-ray source (50 kV, 24 mA, 1.2 kW, and Mo$K\alpha$) with a hybrid pixel array detector and a single-crystal diffractometer, and the following results were obtained: $a = 7.2904(2)$ Å, $c = 3.7686(2)$ Å, $V = 173.47(1)$ Å$^3$, and $Z = 1$. These two experimental results for different grains are similar, but both differ from that of the synthetic material, for which the unit-cell parameter of $c$ is double ($a = 7.23072$ Å, $c = 7.5462$ Å; Weinstock et al., 1999). The final unit-cell parameters were based on 777 reflections, resulting in unit-cell parameters of $a = 7.2952(5)$ Å, $c = 3.7711(3)$ Å, $V = 173.81(2)$ Å$^3$, and $Z = 1$. The space group was obtained using the XPREP software and was assumed to be $P6/mmm$ due to the lack of any systematic extinction.

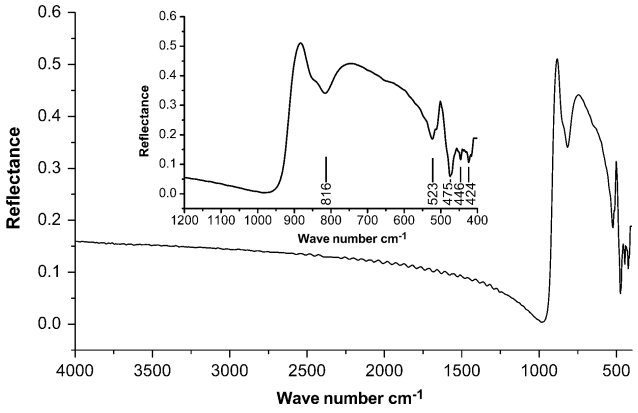


**Figure 4.** The IR spectrum of wumuite.

**Table 2.** X-ray powder diffraction data ($d$ in Å) for wumuite. The four strongest reflections are given in bold.

| $h$ | $k$ | $l$ | $d_{obs}$ | $d_{cal}$ | $I/I_0$ |
|---|---|---|---|---|---|
| **0** | **1** | **0** | **6.261** | **6.309** | **36** |
| **0** | **0** | **1** | **3.727** | **3.767** | **30** |
| **0** | **2** | **0** | **3.161** | **3.154** | **100** |
| 1 | 1 | 1 | 2.610 | 2.618 | 10 |
| **0** | **2** | **1** | **2.413** | **2.418** | **40** |
| 0 | 3 | 0 | 2.107 | 2.103 | 5 |
| 1 | 2 | 1 | 2.015 | 2.014 | 3 |
| 0 | 0 | 2 | 1.881 | 1.883 | 10 |
| 2 | 2 | 0 | 1.820 | 1.821 | 15 |
| 1 | 3 | 0 | 1.748 | 1.749 | 3 |
| 2 | 2 | 1 | 1.632 | 1.639 | 10 |
| 0 | 4 | 0 | 1.577 | 1.577 | 15 |
| 0 | 4 | 1 | 1.455 | 1.454 | 10 |
| 2 | 3 | 1 | 1.355 | 1.351 | 2 |
| 2 | 2 | 2 | 1.311 | 1.309 | 5 |
| 0 | 5 | 1 | 1.196 | 1.196 | 5 |
| 0 | 2 | 3 | 1.168 | 1.166 | 3 |

When the crystal structure of wumuite was initially analyzed, the cell parameters and space group of the synthetic $KAl_{0.33}W_{2.67}O_9$ were first referred to. However, it should be noted that the diffraction data for wumuite were collected at 20 s per frame, and only 38 very weak superlattice diffraction points with an average intensity that was only 1/1000 of that of the strong points were observed in the lower layer (Fig. 5). For this reason, no complete reciprocal cells were obtained, and the parameter $c = 7.4$ Å could not be obtained from the index using the single-crystal diffraction data for wumuite.

Considering that the index using the assigned cell parameters with $c = 7.4$ Å would lack a great deal of diffraction data, as is evident from the single-crystal diffraction reciprocity lattice in Fig. 5, and the systematic extinction characteristics of wumuite do not conform to the extinction law of $P6_3/mcm$, we believe that the natural mineral and the synthetic material are different in terms of the cell parameters

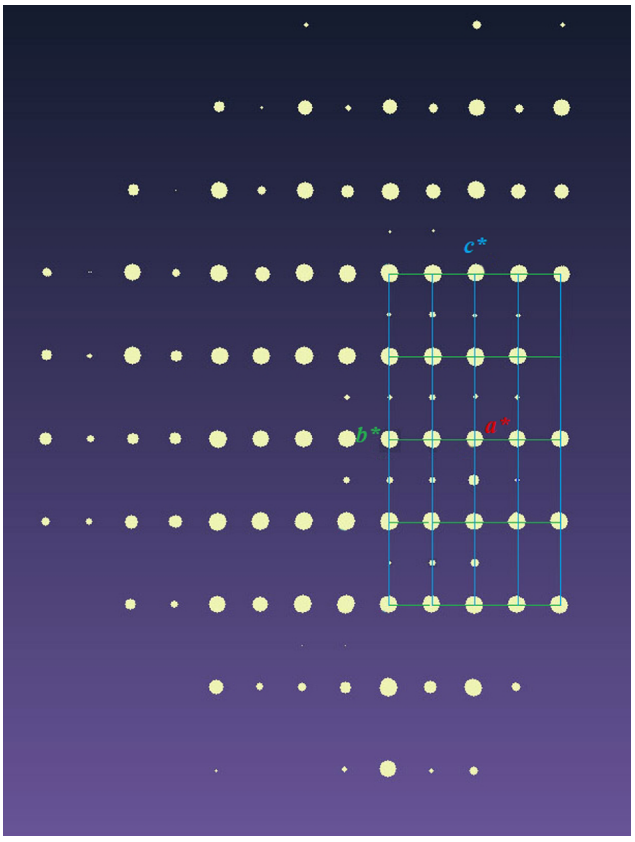


**Figure 5.** Single-crystal diffraction points of wumuite (view along $a^*$).

and space group. The current results are more reasonable for the experimental data obtained using a high-power single-crystal diffractometer. Several of the differences in the patterns of the powder diffraction also provide support. It is possible that the replacement of $W^{6+}$ by $Al^{3+}$ is more disorderly or that the K atoms are displaced from the ideal (0, 0, 1/2) position, resulting in the symmetry of the natural mineral being different from that of the synthetic material.

The structure solution and refinement were determined using the Shelx2014 program. The crystal structure was solved by direct methods. The crystal structure of wumuite refinement led to a reliability factor of $R_1[F^2 > 4\sigma(F^2)] = 0.025$ ($wR_2 = 0.072$) for 164 independent reflections (777 measured reflections, $R_{(int)} = 0.011$). The data collection information and structural refinement details for wumuite are listed in Table 3. The positional parameters, anisotropic displacement parameters, and bond distance parameters are presented in Tables 4, 5, and 6.

Wumuite is a hexagonal tungsten bronze (HTB)-type structure. The layers of corner-sharing $[(W, Al)O]_6$ octahedra, with the layers oriented normal to the short (3.7713 Å) $c$ repeat and along with the W–O–W links, connect them to form a hexagonal ring channel (tunnel). K atoms reside in the tunnel (Figs. 6 and 7a). As shown in Fig. 6b and Ta-

**Table 3.** Crystal data, data collection information, and structural refinement details of wumuite.

| | |
|---|---|
| Simplified formula | $KAl_{0.33}W_{2.67}O_9$ |
| Crystal size | $0.07 \times 0.07 \times 0.05\,mm^3$ |
| Space group | *P6/mmm* |
| Unit-cell parameters | $a = 7.2952(5)$ Å, $c = 3.7711(3)$ Å, $V = 173.81(2)$ Å$^3$ |
| $Z$ | 1 |
| Density (calculated) | $6.52\,g\,cm^{-3}$ |
| Data collection | |
| Diffractometer | CCD detector |
| Radiation, wavelength | Mo$K\alpha$, $\lambda = 0.71073$ Å |
| Measured reflections | 777 |
| Independent reflections | 164 |
| Independent reflections with $I > 2\sigma(I)$ | 162 |
| $R_{int}$ | 0.01 |
| $\theta_{min}$, $\theta_{max}$ | 3.22, 33.03° |
| Index range | $-9 \le h \le 9$, $-10 \le k \le 2$, $-4 \le l \le 5$ |
| Refinement | |
| Refinement method | Full matrix least squares on $F^2$ |
| Data/restraints/parameters | 164/0/14 |
| Goodness of fit on $F^2$ | 1.05 |
| Final $R$ indices $[I > 2\sigma(I)]$ | $R_1 = 0.025$, $wR_2 = 0.072$ |
| $R$ indices (all data) | $R_1 = 0.025$, $wR_2 = 0.072$ |
| Extinction coefficient | |
| Largest different peak and hole | 1.858 and $-1.14\,e\,Å^{-3}$ |

**Table 4.** Atomic coordinates of wumuite.

| Atom | Wyckoff | Occupancy | $x$ | $y$ | $z$ | $U_{eq}$ |
|---|---|---|---|---|---|---|
| K1 | 1*b* | 0.8 | 0 | 0 | 1/2 | 0.120(11) |
| W1 | 3*f* | 0.89 | 0 | 1/2 | 0 | 0.0281(3) |
| Al1 | 3*f* | 0.11 | 0 | 1/2 | 0 | 0.0281(3) |
| O1 | 6*l* | 1 | 0.7894(5) | 0.2106(5) | 0 | 0.044(2) |
| O2 | 3*g* | 1 | 0 | 1/2 | 1/2 | 0.068(8) |

ble 5, the placement of potassium in the big cavities of the tunnels results in high thermal vibration parameters. In the crystal structure, W and Al occupy the same site, and the W–Al substitution is disordered. The (W, Al)–O bond length is 1.886 Å, which is shorter than that of the general W–O bond (1.998 Å). The valence bond analysis is shown in Table 7.

The unit-cell parameters $a$ and $c$ are similar to those of tewite ($a = 7.2585(4)$ Å, $b = 25.8099(15)$ Å, $c = 3.8177(2)$ Å, $V = 715.21(7)$ Å$^3$, orthorhombic, *Pban*), and the structural comparison is shown in Fig. 7. Both wumuite and tewite, another new K–W mineral discovered in the same sample, have modulation structures. In the average structure of tewite, the electron-density concentrations assigned to K occur at K1 (2*a* [0.75 0.75 0]) and K2 (4*k* [0.75 0.75 0.681], subsite), implying that vacancies are necessary to explain the short interatomic distances (Li et al., 2019). Similarly, the close proximity of the K–K sites in wumuite's structure precludes simultaneous occupation, but a simple interchange between sites may be the cause of the high potassium temperature factor. Moreover, the maximum potassium occupancy in hexagonal potassium tungsten bronze is 1/3 approximately, which is determined by the available sites in the hexagonal tunnels.

For synthetic potassium tungsten bronze ($K_xWO_3$) materials, the modulation structure of K is usually related to the isomorphic substitution or the mixed-valence state of the W ions. Theoretically, the charge balance of the chemical formula is satisfied when $x = 0$. Therefore, the doping of K is usually accompanied by the isomorphic substitution of $W^{6+}$ by other ions (e.g., $Al^{3+}$, $K^+ : Al^{3+} = 3 : 1$) or substitution by the same amount of the homoatomic aliovalent ion $W^{5+}$

**Table 5.** Anisotropic displacement parameters ($Å^2 \times 10^3$) of wumuite.

| Atom | $U_{11}$ | $U_{22}$ | $U_{33}$ | $U_{12}$ | $U_{13}$ | $U_{23}$ |
|---|---|---|---|---|---|---|
| K1 | 0.058(5) | 0.058(5) | 0.24(3) | 0.029(2) | 0.00000 | 0.00000 |
| W1 | 0.0187(3) | 0.0254(3) | 0.0381(4) | 0.00934(16) | 0.00000 | 0.00000 |
| Al1 | 0.0187(3) | 0.0254(3) | 0.0381(4) | 0.00934(16) | 0.00000 | 0.00000 |
| O1 | 0.0128(16) | 0.0128(16) | 0.106(7) | 0.0055(18) | 0.00000 | 0.00000 |
| O2 | 0.048(8) | 0.110(17) | 0.024(6) | 0.024(4) | 0.00000 | 0.00000 |

**Table 6.** Selected bond lengths (Å) in wumuite.

| | | |
|---|---|---|
| K1–O1 | ×12 | 3.261(1) |
| K1–O2 | ×6 | 3.648(3) |
| W1–O2 | ×2 | 1.886(0) |
| W1–O1 | ×4 | 1.891(3) |

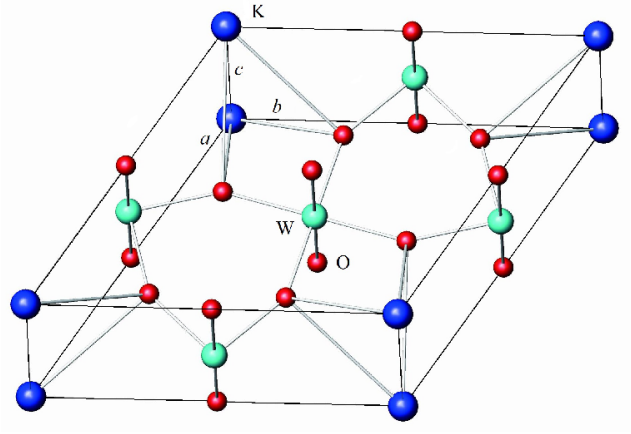


(a)

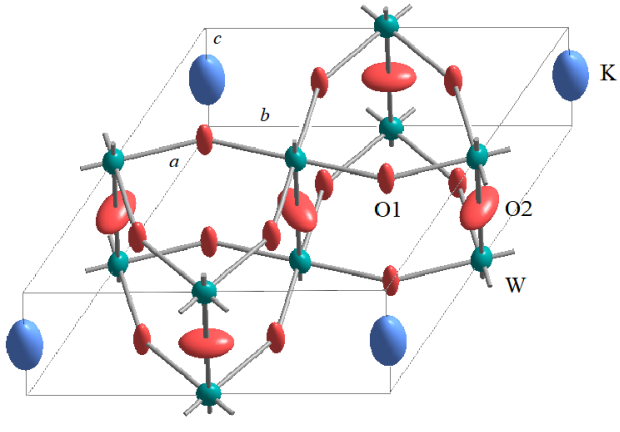


(b)

**Figure 6.** Crystal structure of wumuite. **(a)** General view; **(b)** DIAMOND 3.1 drawing of wumuite with thermal ellipsoid plot (50 % probability).

**Table 7.** Bond-valence analysis of wumuite.

| | W site | K | O sum |
|---|---|---|---|
| O1 | $0.997 \times 4\downarrow, \times 2\rightarrow$ | $0.036 \times 12\downarrow, \times 1\rightarrow$ | 2.030 |
| O2 | $1.015 \times 2\downarrow, \times 2\rightarrow$ | $0.013 \times 6\downarrow, \times 1\rightarrow$ | 2.043 |
| Sum | 6.019 | 0.51 | |

The bond strength for the W site is based on occupancy by $0.89W^{6+} + 0.11Al^{3+}$ and K occupancy by 0.8. The bond-valence calculations were done using the equation and constants of (Brown, 1977) $S = \exp[(R_0 - d_0)/b]$, $Al^{3+}$–O bond parameters from Allmann (1975), $W^{6+}$–O bond parameters from Tytko et al. (1999), and $K^+$–O from Wood and Palenik (1999).

as that of $K^+$ ($K^+ : W^{5+} = 1 : 1$), thereby forming a nonstoichiometric compound.

In wumuite, the nonstoichiometry is caused by the substitution of $W^{6+}$ by $Al^{3+}$. As shown in Table 7, the valence bond calculation was performed using the refined structural data, and the results show that W has a bond valence sum of 6.019 $u.v$. In addition, the experimental chemical formula calculated from the electron microprobe data has a good charge balance. Both of these facts indicate that the crystal structure of wumuite mainly offsets the excessive positive charge brought about by $K^+$ through the substitution of $W^{6+}$ by $Al^{3+}$. Therefore, Al is a characteristic element with a definite proportion in wumuite, and its ideal formula should not be simply written as $K(W, Al)_3O_9$ but rather as $K(W_{2.67}Al_{0.33})_{\Sigma 3}O_9$ or $KAl_{0.33}W_{2.67}O_9$. Guo et al. (2015) pointed out that the higher the valence state and the higher the content of A in the tungsten bronze structure, the more W ions with the lower valence state are needed to balance the local charge in the unit cell, which increases the frequency of the lattice distortion or phase transformation. Similarly, an increase in $Al^{3+}$ will also help the structure to accommodate more $K^+$ and other high-valence A-site ions.

### 6.3 The crystal structure and crystal chemistry

The general formula for oxide bronze compounds is $A_xMO_n$ (Zhou, 1982), where A is a positively charged ion, M is a transition metal ion, and $n$ can be an integer or a noninteger (Guo et al., 2015). The term tungsten bronze compound (TB) refers to a series of compounds whose M site is occupied by tungsten. Since the $x$ value varies within a certain range, there is no definite stoichiometric ratio for the component

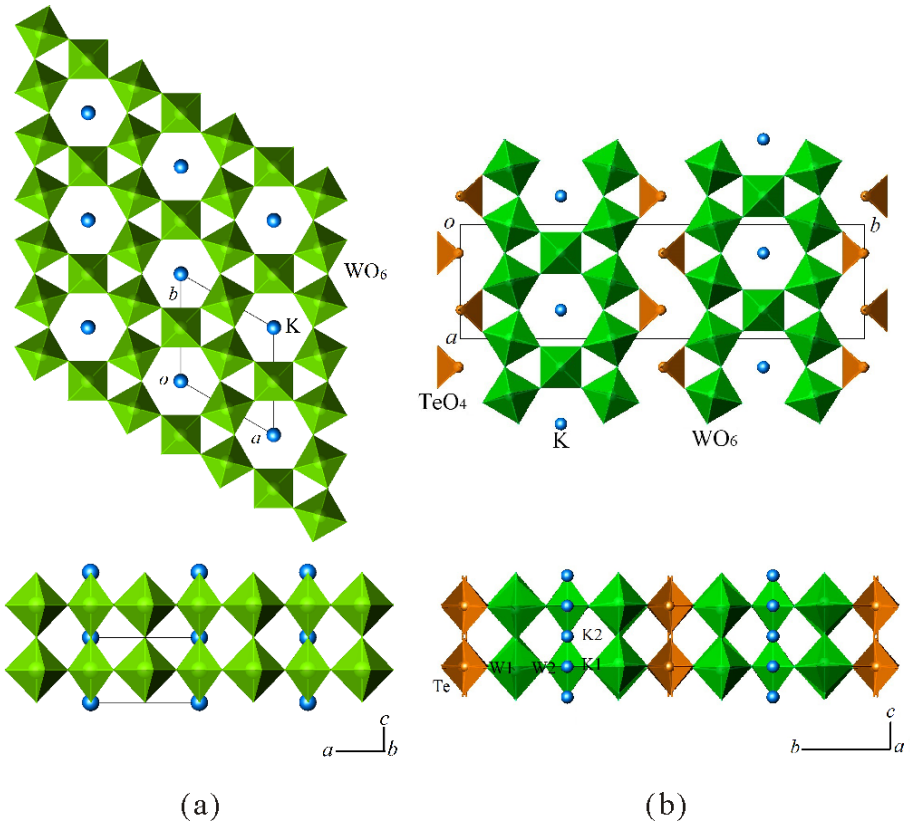


**Figure 7.** Comparison of the structures of **(a)** wumuite and **(b)** tewite.

elements, so TB is a nonstoichiometric compound with the general formula of $A_xWO_3$ ($0 < x < 1$). The crystal structure of tungsten bronze can be regarded as an open framework structure with polyhedron holes formed by regular or distorted $WO_6$ octahedra by corner sharing, and A ions occupy these holes. With the filling with A, homoatomic aliovalent ions of tungsten appear; that is, W becomes a mixed-valence ion (e.g., $W^{6+}$, $W^{5+}$, and $W^{4+}$), thereby forming a nonstoichiometric compound (Guo et al., 2015). Tungsten bronze has a special space tunnel structure, which can be divided into perovskite-type tungsten bronze or cubic tungsten bronze (PTB or CTB), tetragonal tungsten bronze (TTB), hexagonal tungsten bronze (HTB), and intergrowth tungsten bronze (ITB) according to the characteristics of the crystal structure. Since PTB and HTB are often nonstoichiometric compounds, they are combined here into one category, namely, nonstoichiometric tungsten bronze (Su et al., 2006).

The crystal structure of tungsten bronze oxide also changes with the content of A. In general, as $x$ increases, the symmetry of the tungsten bronze crystal's structure gradually increases (Guo et al., 2015). Previous studies have shown that $A_xWO_3$ (A = K, Rb, Cs) forms HTB when $x = 0.19$–$0.33$, but as $x$ decreases ($x < 0.10$), HTB becomes unstable and forms ITB, which is formed through the alternation of the $WO_3$ and HTB layers. Therefore, ITB is also called quasi-two-dimensional tungsten bronze (Qi, 2008).

Based on a comparison of the crystallographic data of potassium tungsten bronze analogues (mainly those with W > K in the chemical formula and that can be doped with Al, $K_x(W, Al)O_3$, $0 < x < 1$) that were previously synthesized or simulated (Table 8), when $0.183 \leq x \leq 0.33$, the materials are mainly hexagonal and can serve as different space groups (Fig. 8a) (wumuite belongs to this category); when $0.37 \leq x \leq 0.57$, it is mainly tetragonal, with space group $P4/mbm$ (Fig. 8b); when $x \approx 0.3$ or $x \approx 0.5$, an orthorhombic system (Fig. 8c) or a cubic system appears. However, based on the cell parameters, neither orthorhombic nor cubic systems are typical tungsten bronze structures.

Although researchers have conducted numerous synthesis experiments and studies of tungsten bronze materials, the natural mineral wumuite still has a different symmetry compared to the artificial synthetic materials. According to the statistics of the diffraction extinction laws, the space group of wumuite is $P6/mmm$, while that of the artificial material is $P6_3/mcm$ (ICDD, 2020b). In addition, wumuite has a $c$ value of 3.77 Å, which is the single-layer thickness of the $WO_6$ octahedral layer (Fig. 7a), that is, the basic type of the $c$ axis of the tungsten bronze structure. In contrast, all of the hexagonal analogues reported by previous researches have a

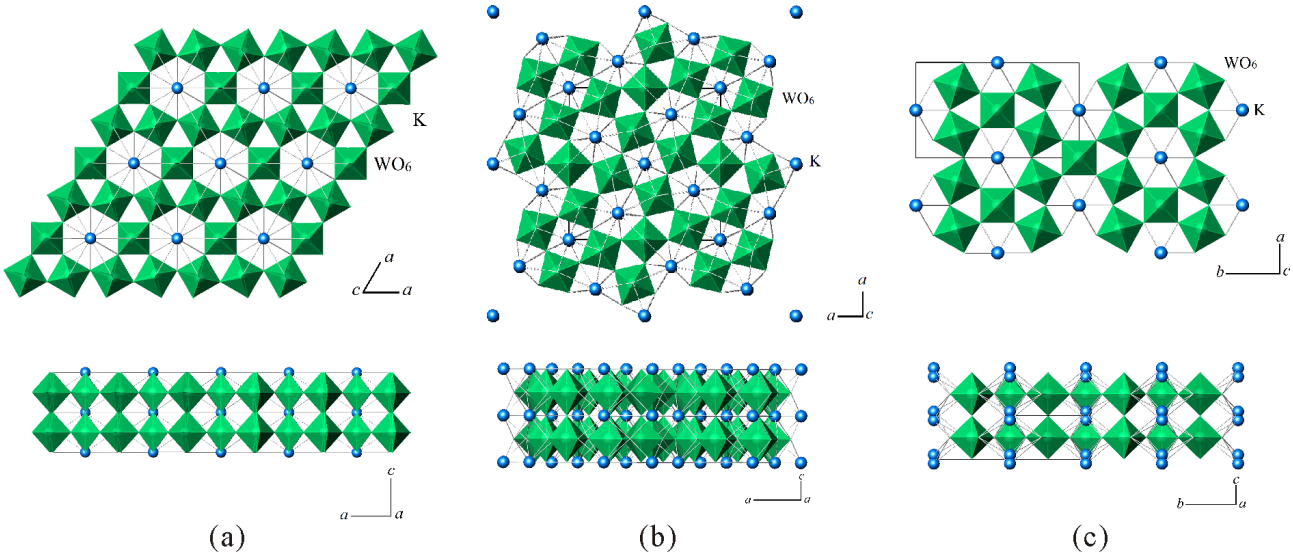


**Figure 8.** Crystal structures of **(a)** hexagonal tungsten bronze (HTB), **(b)** tetragonal tungsten bronze (TTB), and **(c)** orthorhombic tungsten bronze (OTB).

**Table 8.** Comparison between wumuite and related synthetic materials (Xue, 2018).

| $x$ | End formula | Space group | Unit cell (Å) | Crystal system | References |
|---|---|---|---|---|---|
| 0.183–0.33 | $K_{0.33}WO_3$ | $P6_3/mcm$ | ($x = 0.32$) 7.3835; 7.3835; 7.5007 | hexagonal | 1 |
| 0.33 | $KAl_{0.33}W_{2.67}O_9$ | $P6_3/mcm$ | 7.3072; 7.3072; 7.5462 | | 2 |
| 0.33 | $KAl_{0.33}W_{2.67}O_9$ | $P6/mmm$ | 7.2952(5); 7.2952(5); 3.7711(3) | | wumuite |
| 0.20–0.26 | $K_{0.26}WO_3$ | $P6_322$ | ($x = 0.26$) 7.385; 7.385; 7.53 | | 3 |
| 0.26 | $K_{0.26}WO_3$ | $P6_3$ | 7.389; 7.389; 7.508 | | 4 |
| 0.33 | $K_{0.33}WO_3$ | $P\bar{6}2m$ | 7.34; 7.34; 7.52 | | 5 |
| 0.33 | $K_{0.33}WO_3$ | $Cmmm$ | 7.302; 12.713; 3.627 | orthorhombic | 6 |
| 0.37–0.57 | $K_{0.57}WO_3$ | $P4/mbm$ | ($x = 0.37$) 12.2605; 12.2605; 3.8259 | tetragonal | 7 |
| 0.5 | $KAl_{0.33}W_{1.67}O_6$ | $Fd\bar{3}m$ | 10.1808; 10.1808; 10.1808 | cubic | 8 |

$x$ represents the coefficient of K and is calculated on the basis of $O_{apfu} = 3$.
References: 1 – Kihlborg and Hussain (1979); 2 – ICDD (2020b); 3 – Pye and Dickens (1979); 4 – Schultz et al. (1986); 5 – ICDD (2020a); 6 – Klug (1977); 7 – Kihlborg and Klug (1973); 8 – Thorogood et al. (2009).

$c$ value of 7.5 Å, i.e., approximately two times that of wumuite (Fig. 8a). These studies revealed that, in the absence of Al, the doubling of the $c$ value is mainly caused by the displacement of tungsten or oxygen atoms. The mechanisms proposed in the references mainly include the following.

1. *The off-center displacement of W atoms.* In $K_{0.32}WO_3$ (space group $P6_3/mcm$), Kihlborg and Hussain (1979) reported that all of the tungsten atoms in one layer of octahedra are at the same $z$ level but are slightly displaced in the $xy$ plane with the deviation of $x$ coordinates from $1/2$, causing the $c$ axis to extend over two layers.

2. *The displacement of O atoms.* The new structural feature found by Pye and Dickens (1979) in $K_{0.26}WO_3$ (space group $P6_322$) is a puckered ring of six O2 atoms forming the "windows" of the hexagonal tunnels. The six window oxygens are sited alternately in two planes perpendicular to the $c$ axis above and below the $z = 0$ level respectively. Similarly, the structural features revealed by Schultz et al. (1986) in $K_{0.26}WO_3$ (space group $P6_3$) are the displacements of O(1A) and O(1B) atoms from $z = 1/4$ with $z$ coordinates differing by $\pm c/20$, although in space group $P6_322$ O(1A) and O(1B) are related by a twofold symmetry axis, whereas in $P6_3$ this constraint is removed.

3. *The contribution from K atoms.* In $K_{0.32}WO_3$ (space group $P6_3/mcm$), the occupancy and temperature factors indicate that the potassium atoms do not occupy the position ($2b$) at the center of the hexagonal tunnels but are distributed throughout other positions in the hexagonal tunnels, probably more or less randomly (Kihlborg

and Hussain, 1979). In $K_{0.26}WO_3$ (space group $P6_322$), the potassium ions appear to be disordered over two sites in the tunnels, towards one of the two sets of window oxygen atoms (Pye and Dickens, 1979). Thus, in the structure of potassium HTB analogues with a doubled *c* parameter, the position of K is more disordered than expected. Nevertheless, based on the different cases, we also concluded that the K atoms are likely to impact the placements of the W, Al, and O atoms in the structure of potassium tungsten bronze materials (Kihlborg and Hussain, 1979; Schultz et al., 1986; Thorogood et al., 2009).

Comparing to the above three cases, there is a certain difference between the structural models of wumuite and the synthetic HTB materials. The symmetry of our present space group $P6/mmm$ requires oxygen and tungsten atoms to be coplanar perpendicular to the *c* axis respectively, and the tungsten atoms should not have obvious deviations on the *xy* plane. In wumuite, the A site may be partially occupied and is probably displaced, which has also been proposed by Kihlborg and Hussain (1979) in potassium tungsten bronze compounds. This is supported by the high potassium temperature factor (Fig. 6b and Table 5) and the fact that the shortest K–O distance for the symmetrical 18-coordinated site in wumuite is 3.261 Å, which is about 0.26 Å longer than the sum of the effective ionic radii of $K^+$ and $O^{2-}$ (Shannon, 1976). Thus, it is concluded that the Wyckoff position 1*b* represents only an average situation, and the cation in the big cavities of the tunnels is displaced from the ideal position, giving rise to more realistic K–O distances (3.26 and 3.64 Å) and a high coordination number (XVIII). The W–O distances in the $WO_6$ octahedra of wumuite vary between 1.886 and 1.891 Å, the difference between which is much smaller than that between 1.846 and 1.998 Å in $K_{0.26}WO_3$ (space group $P6_322$; Pye and Dickens, 1979), indicating that the $WO_6$ octahedra in wumuite are only slightly distorted. Due to the substitution by aluminum, the observed (W, Al)–O bond length is 1.886 Å, which is appreciably shorter than the general W–O bond length (1.998 Å).

The presence of satellite reflections in the X-ray diffraction patterns obtained for wumuite in this study may be due to a superlattice structure involving K vacancies, the modulation of the O atoms, and especially the ordering between W and Al in the octahedral sites. However, the quantity and the intensity of the observed satellite reflections were too limited to confirm the existence of superstructures. Actually, for potassium tungsten bronze compounds, the X-ray data are dominated by the scattering from the W atoms. Schultz et al. (1986) pointed out that, without the neutron diffraction results, space group $P6_3/mcm$ for synthetic $K_{0.32}WO_3$ could not be easily disputed, which is because the satellite reflections observed using X-ray diffraction are very weak. The structures of this type of material have been investigated widely using X-ray and neutron powder diffraction methods. In the future, more effective results may be obtained using neutron powder diffraction to study the structure of wumuite, which is prevented by the rarity of natural mineral samples at present.

## 7 Discussion of the genesis of wumuite

Base on the above discussions, although wumuite is the only natural potassium tungsten bronze mineral found in nature, from the perspective of synthetic materials, there will be a great deal of similar potential new minerals as a result of the variations in the chemical components and crystal structure. Therefore, the rarity of such a natural mineral is probably caused by the fact that its formation requires a special geological environment. Why have a series of minerals containing K, Te, and W, such as wumuite, tewite, tellurite, scheelite, and natural $WO_3$, been found in monzonite near gold mines? This is a matter of concern, so we investigated the genesis of these minerals.

Field investigations and laboratory studies have shown that these minerals are related in terms of their genesis and are associated with nearby gold mines. Moreover, these minerals may be formed by a hydrothermal fluid rich in tellurium and tungsten intercalating into the monzonite and reacting with potassium feldspar (orthoclase) during the gold mineralization (Li et al., 2018). We suspect that the formation process of these minerals may be divided into two different reaction process stages as follows.

Step 1:

$$\underset{\text{Orthoclase}}{KAlSi_3O_8} + \underset{\text{Natural } WO_3}{WO_3} \rightarrow \underset{\text{Wumuite}}{KAl_{0.33}W_{2.67}O_9} + \underset{\text{Quartz}}{SiO_2}$$

Step 2:

$$\underset{\text{Wumuite}}{KAl_{0.33}W_{2.67}O_9} + \underset{\text{Natural } WO_3}{WO_3} + \underset{\text{Tellurite}}{TeO_2} \rightarrow \underset{\text{Tewite}}{K_{1.5}(Te,W)_{1.5}W_5O_{19}} + \underset{\text{Corundum}}{Al_2O_3}$$

In order to verify the formation process above, we conducted artificial synthetic experiments. First, wumuite was successfully synthesized from pure $WO_3$ and natural potassium feldspar (orthoclase) from granite under the conditions of atmospheric pressure and 700 °C (Fig. 9a). Then, tewite was obtained by mixing synthetic wumuite with $WO_3$ and $TeO_2$, followed by heating for 10 h at 650 °C and atmospheric pressure, as well as natural cooling to room temperature (Fig. 9b).

These two reactions indicate that wumuite is likely formed by the reaction between potassium feldspar in the monzonite and $WO_3$ from ore fluids at high temperatures, and the allotriomorphic tewite around the wumuite crystals may be the

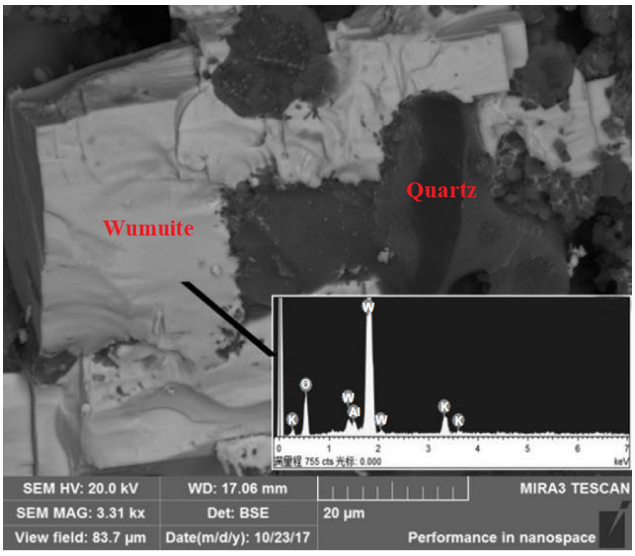


(a)

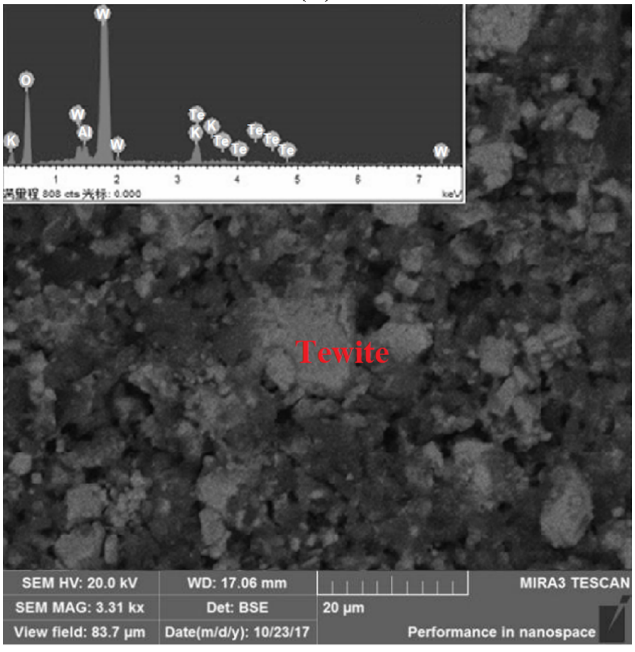


(b)

**Figure 9.** The BSE images of the products of the artificial synthetic experiments. **(a)** Wumuite was synthesized from $WO_3$ and natural potassium feldspar; **(b)** tewite was synthesized from $WO_3$, $TeO_2$, and the synthetic wumuite.

product of the reaction between wumuite and the slightly-lower-temperature fluids of the gold mineralization stage, which were rich in W and Te.

Therefore, it is speculated that these new minerals may have been generated from the reaction between a high-temperature vapor–liquid rich in Te and W and the potassium feldspar and other potassium-bearing minerals in the quartz monzonite in the early stage of gold mineralization, followed by intercalation into the rock mass at the edge of the quartz monzonite.

## 8 Implications

Wumuite is another new mineral containing potassium and tungsten discovered in the Pan–Xi region after tewite was discovered. It is also a natural mineral with a tungsten-bronze-type structure discovered for the first time. Synthetic tungsten bronze materials have attracted extensive attention due to their excellent ferroelectric, piezoelectric, pyroelectric, and nonlinear optical properties. The natural mineral found in this study has the same structure type as synthetic tungsten bronze materials but has different cell parameters and space groups. The discovery of natural tungsten bronze minerals provides a new scientific basis for the recognition and utilization of new substances in nature and the synthesis of functional materials. At the same time, the series of new W and K minerals found in this area in recent years proves the existence of tungsten bronze oxide minerals in the natural metallogenetic environment. Moreover, as this type of synthetic material has a relatively in-depth research basis, its formation conditions can be determined based on its chemical composition and crystal structure. This will provide evidence for the study of the physical and chemical conditions required for the formation of mining areas and has important geological significance for the study of mineral genesis and geological processes.

*Data availability.* All data are available upon request to Guowu Li (liguowu@cugb.edu.cn).

*Author contributions.* YuX and GL designed the experiments and YuX and YiX carried them out. GL performed the structural determination and refinement. YuX prepared the manuscript with contributions from all coauthors.

*Competing interests.* The authors declare that they have no conflict of interest.

*Acknowledgements.* We thank Sergey Krivovichev, Paola Comodi, Daniel Atencio, and an anonymous reviewer for their constructive comments on the manuscript. We thank Ulf Hålenius and anonymous referees for their valuable suggestions on wumuite. We also thank Chen Delin for his assistance during the field work and Ge Xiangkun (Beijing Research Institute of Uranium Geology) for the chemical analysis. We thank LetPub (https://www.letpub.com/, last access: 10 August 2020) for its linguistic assistance during the preparation of the manuscript.

*Financial support.* This research has been supported by the National Natural Science Foundation of China (grant no. 41672043) and the China National Postdoctoral Program for Innovative Talents (grant no. BX20190304).

*Review statement.* This paper was edited by Paola Comodi and reviewed by Daniel Atencio and one anonymous referee.

## References

Allmann, R.: Relations between bond lengths and bond strengths in oxide structures, Monatsh. Chem., 106, 779–793, 1975.

Brown, I. D.: Predicting Bond Lengths in Inorganic Crystals, Acta Crystallogr., B33, 1305–1310, 1977.

Chen, Y. C., Yin, J. Z., Zhou, J. X., Mao, J. W., Yang, B. C., and Luo, Y. N.: Geological Characteristics of Dashuigou Tellurium Ore deposit in Shimian Country, Sichuan Province, China, Sci. Geol. Sinica, 29, 165–167, 1994.

Gadsden, J. A.: Infrared spectra of minerals and related inorganic compounds, Butterworth, London, England, p. 152, 1975.

Guo, J., Lu, X. F., Gao, C. J., and Hou, X. Q.: Effects of element A on the crystal structure of tungsten bronzes $A_xWO_3$, J. Funct. Mater., 17, 17008–17013, 2015.

He, J. L.: Ore-forming Geological Conditions and Prospecting Potential for Nb–Ta Mineral Deposits in Panzhihua-Xichang Region, Sichuan, Acta Geol. Sichuan, 24, 206–211, 2004.

International Centre for Diffraction Data (ICDD): PDF 26-1340, available at: http://icdd.mybigcommerce.com/, last access: 2 Septemper 2020a.

International Centre for Diffraction Data (ICDD): PDF 49-407, available at: http://icdd.mybigcommerce.com/, last access: 2 Septemper 2020b.

Kihlborg, L. and Hussain, A.: Alkali metal location and tungsten off-center displacement in hexagonal potassium and cesium tungsten bronzes, Mater. Res. Bull., 14, 667–674, 1979.

Kihlborg, L. and Klug, A.: Alkali metal distribution in tetragonal potassium tungsten bronze structure, Chem. Scr., 3, 207–211, 1973.

Klug, A.: X-ray diffraction studies of potassium polytungstates with high $WO_3$ content, Mater. Res. Bull., 12, 837–845, 1977.

Li, G. W., Xue, Y., and Xie, Y. M.: Mineralogical characteristics and genesis of new mineral tewite, Bull. Mineral., Petrol. Geochem., 37, 186–191, 2018.

Li, G. W., Xue, Y., and Xiong, M.: Tewite: A K-Te-W new mineral species with a derived structure of hexagonal tungsten bronze, from Panzhihua–Xichang region, Southwest of China, Eur. J. Mineral., 31, 145–152, 2019.

Li, L. Z.: Geologic features and exploitation perspective of REE ore deposits in Panzhihua–Xichang region, Acta Geol. Sichuan, 12, 150–152, 2001.

Pye, M. F. and Dickens, P. G.: A structural study of the hexagonal potassium tungsten bronze, $K_{0.26}WO_3$, Mater. Res. Bull., 14, 1397–1402, 1979.

Qi, B.: Fabrication and research on properties materials of the strontium barium niobate ceramic, Ph.D. thesis, Guilin University of Electronic Technology, Guilin, China, 2008.

Qin, Z.: Metallognetic conditions and prospecting perspective for ore deposits of rare metals and REE associated with alkali series in Panzhihua–Xichang region, Acta Geol. Sichuan, 15, 102–112, 1995.

Schultz, A. J., Horiuchi, H., and Krause, H. B.: Time-of-flight single-crystal neutron and X-ray diffraction study of $K_{0.26}WO_3$, Acta Crystallogr., C42, 641–644, 1986.

Shannon, R. D.: Revised effective ionic radii and systematic studies of interatomic distances in halides and chalcogenides, Acta Crystallogr., A32, 751–767, 1976.

Su, M. H., Li, Z. H., Wei, Y. D., Li, X., and Zhou, B. B.: Study on tungsten bronzes $M_xWO_3$, J. Harbin Inst. Technol., 88, 92–173, 2006.

Thorogood, G. J., Peterson, V. K., Kennedy, B. J., Hanna, J. V., and Luca, V.: Anomalous lattice parameter increase in alkali earth aluminium substituted tungsten defect pyrochlores, J. Solid State Chem., 182, 457–464, 2009.

Tytko, K. H., Mehmke, J., and Kurad, D.: Bond length–bond valence relationships with particular reference to polyoxometalate chemistry, Struct. Bonding, 93, 1–66, 1999.

Weinstock, I. A., Cowan, J. J., Barbuzzi, E. M. G., Zeng, H., and Hill, C. L.: Equilibria between alpha and beta isomers of Keggin heteropolytungstates, J. Am. Chem. Soc., 121, 4608–4617, 1999.

Wood, R. M. and Palenik, G. J.: Bond valence sums in coordination chemistry using new $R_0$ values. Potassium–oxygen complexes, Inorg. Chem., 38, 1031–1034, 1999.

Xu, Y. G., Luo, Z. Y., Huang, X. L., He, B., Long, X., Xie, L. W., and Shi, Y. R.: Zircon U-Pb and Hf isotope constraints on crustal melting associated with the Emeishan mantle plume, Geochim. Cosmochim. Acta, 72, 3084–3104, 2008.

Xue, Y.: Study on Accessory Minerals in Alkaline Rocks in Pan–Xi Region, Ph.D. thesis, China University of Geosciences (Beijing), Beijing, China, 2018.

Zhang, C. J., Liu, J. D., Liu, X. F., Li, Y. G., and Yang, Z. X.: Metallization systems in the Panzhihua–Xichang area of Sichuan, China, J. Chengdu Univ. Technol. (Sci. Technol. Ed.), 36, 387–394, 2009.

Zhong, H., Zhu, W. G., Chu, Z. Y., He, D. F., and Song, X. Y.: Shrimp U-Pb zircon geochronology, geochemistry, and Nd-Sr isotopic study of contrasting granites in the Emeishan large igneous province, Chem. Geol., 236, 112–133, 2007.

Zhou G. D.: Inorganic structure chemistry, Science Press, Beijing, China, 1982.